Energy Storage Materials 29 (2020) 361–366

Contents lists available at ScienceDirect

Energy Storage Materials

journal homepage: www.elsevier.com/locate/ensm

Bifunctional composite separator with a solid-state-battery strategy for dendrite-free lithium metal batteries

Hanyu Huo [a,b], Xiaona Li [a], Yue Chen [b], Jianneng Liang [a], Sixu Deng [a], Xuejie Gao [a], Kieran Doyle-Davis [a], Ruying Li [a], Xiangxin Guo [c,***], Yang Shen [d], Ce-Wen Nan [d,**], Xueliang Sun [a,*]

[a] Department of Mechanical and Materials Engineering, University of Western Ontario, Ontario, N6A 5B9, Canada
[b] State Key Laboratory of High Performance Ceramics and Superfine Microstructure, Shanghai Institute of Ceramics, Chinese Academy of Sciences, Shanghai, 200050, China
[c] College of Physics, Qingdao University, Qingdao, 266071, China
[d] School of Materials Science and Engineering, State Key Lab of New Ceramics and Fine Processing, Tsinghua University, Beijing, 100084, China

ARTICLE INFO

Keywords:
Separators
Solid-state-battery strategies
Highly conductive Li^+ pathways
Garnets
Li metal batteries

ABSTRACT

Lithium (Li) metal anodes have been considered as the "Holy Grail" for next-generation batteries due to their high theoretical capacity and low redox potential. However, nonuniform Li^+ deposition leads to hazardous dendrite growth and poor electrochemical performance, which still severely hinders the practical applications of Li metal batteries. Herein, we propose a bifunctional composite separator to guide homogenous Li^+ deposition, which smartly learns abundant experience from the dendrite-free design of solid-state batteries. A hierarchical porous composite solid-state electrolyte (CSE) consisting of polyvinylidene fluoride (PVDF) and $Li_{6.4}La_3Zr_{1.4}Ta_{0.6}O_{12}$ (LLZTO) is coated on one side of polypropylene (PP) separator to fabricate the composite separator. The interactions between PVDF and LLZTO provide a three-dimensional fast Li^+ channel along the PVDF, LLZTO, and PVDF/LLZTO interfaces, which can effectively redistribute uneven Li^+ flux coming from the insulated PP separator. In addition, the CSE layer can further immobilize the anions, regulating a facile Li^+ transport to evenly deposit on the Li anode. The synergetic effects between Li^+ redistribution and anion immobilization result in higher Coulombic efficiency and enhanced cycling stability for Li metal batteries. This work presents fresh insights into CSE modified PP separator, which is an effective and simple solid-state-battery strategy for protected Li metal anodes and large-scale production.

1. Introduction

Today, advanced energy-storage systems with improved energy density are pursued worldwide as the push for long-lasting electric vehicles and portable electronics increases year over year. However, current lithium-ion batteries (LIBs) are far from the energy density required due to the limited specific capacity of widely used commercial graphite anodes. Lithium (Li) metal possesses an extremely high theoretical capacity (3860 mAh g^{-1}, 10 times larger than graphite anodes), low negative electrochemical potential (−3.04 V vs. the standard hydrogen electrode), and light weight (0.53 g cm^{-3}), leading to its viewing as the "Holy Grail" anode [1,2]. Li metal anodes can be constructed with sulfur or oxygen cathodes to deliver further enhanced energy density for next-generation energy storage technologies [3,4].

Nevertheless, hazardous Li dendrite growth in working batteries still hinders the practical application of Li metal anodes. The components in liquid electrolytes tend to be spontaneously reduced due to the highly reactive nature of Li, forming solid electrolyte interphase (SEI) on the surface of Li anodes. The as-formed SEI is mechanically brittle and chemically heterogeneous during the stripping/plating process, which exposes the fresh Li to continuous reactions with the electrolyte [5]. It not only decreases the Coulombic efficiency of working batteries by irreversibly consuming the Li metal but also increases the microscopic roughness of Li surface. The rough Li surface inevitably gives rise to the

* Corresponding author.
** Corresponding author.
*** Corresponding author.
E-mail addresses: xxguo@qdu.edu.cn (X. Guo), cwnan@mail.tsinghua.edu.cn (C.-W. Nan), xsun9@uwo.ca (X. Sun).

https://doi.org/10.1016/j.ensm.2019.12.022
Received 19 October 2019; Received in revised form 18 November 2019; Accepted 12 December 2019
Available online 17 December 2019

uneven Li^+ flux and undesirable dendritic Li nucleation. Moreover, once tiny Li dendrites nucleate, the Li will be preferentially deposited on the top of the protuberant tips with the rapidly changing electronic field, thus Li dendrite propagation resulting in cell life-span reduction and eventual termination [6].

Intensive efforts have been devoted to addressing the dendrite issue in Li metal batteries. Electrolyte additives have been used to modify the chemical components of SEI by *in-situ* forming an artificial SEI on the surface of Li metal [7]. *Ex-situ* coating layers have also been deposited on the surface of Li metal to protect Li against dendrite growth, including ultrathin inorganic layers and polymer thin films [8,9]. Three-dimensional (3D) Li matrices show a high specific surface area, which can effectively lower the local current density, thus extending the Sand's time [10]. These strategies based on the component and structural modifications of Li anodes provide fresh insights into high-safety battery design with dendrite-free Li anodes.

As an important part of cells, separators play a critical role in determining the cell's electrochemical performance. It is believed that separator modification is more convenient than Li metal anode modification to achieve stable Li plating/stripping. In recent years, separators with various surface modifications have been reported. Most of them mainly focus on the improvement of thermal stability at an elevated temperature, electrochemical stability at a high voltage, wettability against electrolytes, and mechanical strengthening [11]. The coating materials included ceramics such as SiO_2, MgO and Al_2O_3, and polymers such as Polyvinylidene Fluoride (PVDF) and siloxy-polymers [12–14]. Only a few studies related to separators for Li dendrite suppression can be found. Cui reported a bifunctional separator, which can detect the internal shorting at the early stage [15]. Some nonconductive materials such as Kimwipe paper, cellulose and mussel-inspired polydopamine were also used to cover separators to suppress Li dendrites [16–18]. These strategies focus on preventing dendrite proliferation and growth, including enhancing the mechanical strength of composite separators, decreasing the pore sizes of coating layers, and killing dendrite by reacting with Li [16,19]. However, the essentially inhomogeneous Li^+ flux that leads to dendrite nucleation is not addressed, thus limiting the improvements of electrochemical performance.

Li^+ transportation in the electrolytes is usually regarded as the rate-determining step of the Li^+ deposition process due to the much slower speed compared with the charge transfer at the electrode [20,21]. Schematic 1a shows that when the Li^+ passes across the separator, it is all trapped in the small separator pores due to the ionically insulating separator skeleton [22]. After passing through the separator, the crowded Li^+ tends to be aggregated near the pores. The anisotropic distribution of Li^+ leads to an aggregated Li^+ deposition at the anode, especially under high current density. Even worse, the migration of active Li^+ can be hindered by the free anions moving in the opposite direction, further aggravating the uneven Li^+ flux [23]. Therefore, a strong space charge forms near the Li anodes, which results in Li dendrite growth and the eventual short circuit of the cells. In this context, if Li^+ can smoothly and uniformly pass through the separator and transport to the Li surface without the interference of anions, a dendrite-free Li metal battery with long-term electrochemical stability can be highly expected.

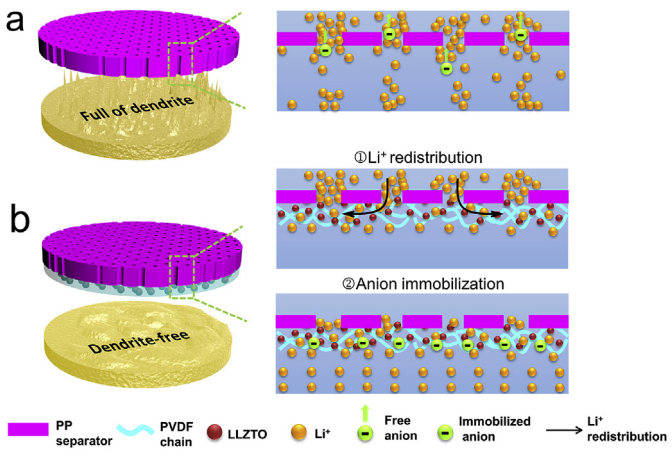

Schematic 1. Schematic illustrations of the Li^+ deposition behaviors through a) PP separator and b) anion-immobilized PP@PLLZ separator with multiple highly-conductive ion pathways.

Herein, a composite-solid-electrolyte (CSE) modified polypropylene (PP) separator is proposed to achieve dendrite-free Li anodes by guiding uniform Li^+ transportation in the liquid electrolyte (Schematic 1b). It's a novel method that taking advantage of solid-state batteries (SSBs) to address the dendrite issue in liquid-based cells. The flexible CSE layers by blade casting can well inherit the excellent flexibility of commercial PP separators, which is good for practical application and large-scale production. In comparison, the single ceramic particles coated on separators by vacuum filtration limited the intrinsic flexibility of separators due to the poor adhesion between ceramic particles and separators [22,24]. The CSE layer consisting of polyvinylidene fluoride (PVDF) and $Li_{6.4}La_3Zr_{1.4}Ta_{0.6}O_{12}$ (LLZTO) (abbreviated as PLLZ) showed an exceptional ionic conductivity (1.4×10^{-4} S cm^{-1} at 25 °C) and a high Li^+ transference number (t_+, 0.66). The multiple three-dimensional (3D) fast Li^+ channels in the PLLZ layer can effectively redistribute the uneven Li^+ flux and guide homogenous deposition. In addition, the high t_+ of the PLLZ layer can fix the free anions released by Li salts, further controlling the Li^+ concentration gradient. Due to the synergetic effect between Li^+ redistribution and anion immobilization, both Li symmetric cells and $LiFePO_4$/Li cells with the modified separators exhibited enhanced cycle stability and extended life span.

2. Results and discussion

The PLLZ layer consists of PVDF polymer, LLZTO particle, and $LiClO_4$ salt. PVDF can effectively dissociate the Li salt due to the high polarization. It also shows low reactivity and high stability in commonly used electrolytes [25]. LLZTO is one of the most promising solid-state fast Li^+ conductors, exhibiting high ionic conductivity and excellent chemical stability [25,26]. The LLZTO powder showed a pure cubic garnet structure with a particle size of ~200 nm in Fig. S1 [27]. The solvent used here was dimethyl formamide (DMF), which exhibited good wettability against the PP separator. The electrolyte slurry was uniformly coated on one side of the PP separator with a blade to form the modified separator (PP@PLLZ) (Fig. S2). Then, the coated separator was immersed in ethanol for solvent exchange followed by vacuum freeze drying under −40 °C for 12 h. This solvent exchange process is good for creating a 3D porous structure for Li^+ migration, which was introduced in our previous works [28,29]. Note that water as a traditional solvent was substituted for ethanol here because of the H^+/Li^+ ion exchange between H_2O and LLZTO particle and the poor wettability of H_2O against the PP separator [30]. The as-obtained PP@PLLZ separator can be rolled around a finger or even twisted into a deformed state without any detachment and cracking, indicating excellent flexibility for flexible electronics (Fig. 1a).

As the X-Ray Diffraction (XRD) pattern shown in Fig. 1b, the diffractions peaks at $2\theta = 14$, 16.9, and 18.6° corresponded to the (110), (040), and (130) crystal planes of the bare PP separator [31]. All components of PLLZ were well integrated into a PP matrix without losing their crystalline structure. The Fourier Transform Infrared Spectroscopy (FTIR) spectra further confirmed the chemical stability between PP separator and the PLLZ coating layer (Fig. S3). The scanning electron microscopy (SEM) image in Fig. S4 shows many large pores on the PP separator, which are mainly distributed on a 2D plane. When coating the PLLZ layer, the PP@PLLZ separator demonstrated a 3D porous structure (Fig. 1c). This could be attributed to the phase inversion by the solvent exchange process [28]. The 3D porous structure can enhance the wettability of modified separators with liquid electrolytes and promote homogenous Li^+ distribution. The cross-sectional SEM image showed

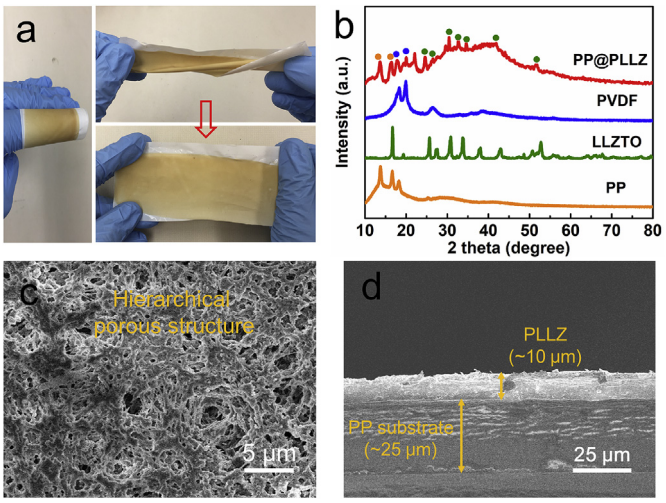

Fig. 1. a) Digital images of bendable PP@PLLZ separator. b) XRD patterns of PP separator, LLZTO, PVDF, and PP@PLLZ separator. c) Top-view and d) cross-sectional SEM images of PP@PLLZ separator.

that the thickness of PLLZ layer was approximately 10 μm and adhered closely to the surface of PP separator (Fig. 1 d).

The feasibility of the PP@PLLZ separators for Li metal anodes was investigated by Li/Cu half cells. A certain amount of Li metal is plated onto the Cu foil which has no Li at the initial state, followed by stripping the Li from Cu substrate to a cut-off voltage, for total Li removal. Coulombic efficiency is defined as the ratio of the stripped Li versus the plated Li metal, which is an indicator to measure the stability of Li plating/stripping behavior [32]. As shown in Fig. 2a, the Li/Cu cells with the unmodified PP separator exhibited poor stability with CE dropping to 86.7% within only 170 cycles at 1 mA cm^{-2} (1 mAh cm^{-2}), while the cells with PP@PLLZ separator demonstrated a steady CE over 97.5% for 300 cycles. The charge and discharge curves at the 100th and 200th cycles in Fig. 2b also showed large voltage hysteresis and obvious fluctuations for the cells with bare PP separator, indicating the inferior electrochemical cycling properties. This could be ascribed to the depletion of both electrolyte and Li metal by continuous breakdown/repair of SEI [33]. In contrast, the cells with PP@PLLZ separator exhibited enhanced electrochemical deposition with a smaller voltage hysteresis (Fig. 2c). When increasing the capacity from 1 to 3 mAh cm^{-2}, the CE and lifespan of the Li/Cu cells with PP separator were even lower (Fig. S5). The PP@PLLZ separator was able to achieve higher Coulombic efficiency and longer cycle life of Li/Cu cells at 3 mAh cm^{-2} compared to the bare PP separator (Fig. S5).

To further investigate the advantage of the PP@PLLZ separator in the cycling stability of Li metal anodes, Li symmetric cells with PP@PLLZ and bare PP separators were assembled, respectively. As shown in Fig. 2d, the PP@PLLZ delivered long-term cycle stability over 1000 h under 1 mA cm^{-2} (1 mAh cm^{-2}). The near-constant overpotential was as low as 40 mV, which could be ascribed to the restrained Li^+ concentration gradient and rapid Li^+ migration at the interface achieved by the PLLZ layer [34]. In contrast, the overpotential of PP separator was initially maintained at ~47 mV for 300 h and gradually increased to over 200 mV after 600 h. The voltage hysteresis resulted from the continuous consumption of electrolyte and Li dendrite growth. Longer galvanostatic time of 3 h (3 mAh cm^{-2}) was further examined in Li symmetric cells at 1 mA cm^{-2}. A short circuit occurred in cells with PP separator after 360 h cycling, while the cells with PP@PLLZ can stably operate over 600 h with a steady overpotential (Fig. S6). Even at higher current densities of 3 mA cm^{-2}, the cells with PP separator exhibited fluctuations in overpotential followed by a sudden drop after only 70 h, indicating short circuit of cells due to rapid Li dendrite growth (Fig. S7). The cells with PP@PLLZ separator can cycle 8.5 times longer time than the ones with PP separator, indicating the excellent capability of dendrite suppression (Fig. S7).

Electrochemical impedance spectroscopy (EIS) and SEM were carried out to provide more insight on cell performance. Fig. 2e and f shows the EIS spectra of cells with PP and PP@PLLZ separators after 200, 400 and 600 h cycling at 1 mA cm^{-2}, respectively. Here, the initial point of the spectra corresponded to the resistance of the bulk electrolyte, while the following semicircle corresponded to the interfacial resistance of

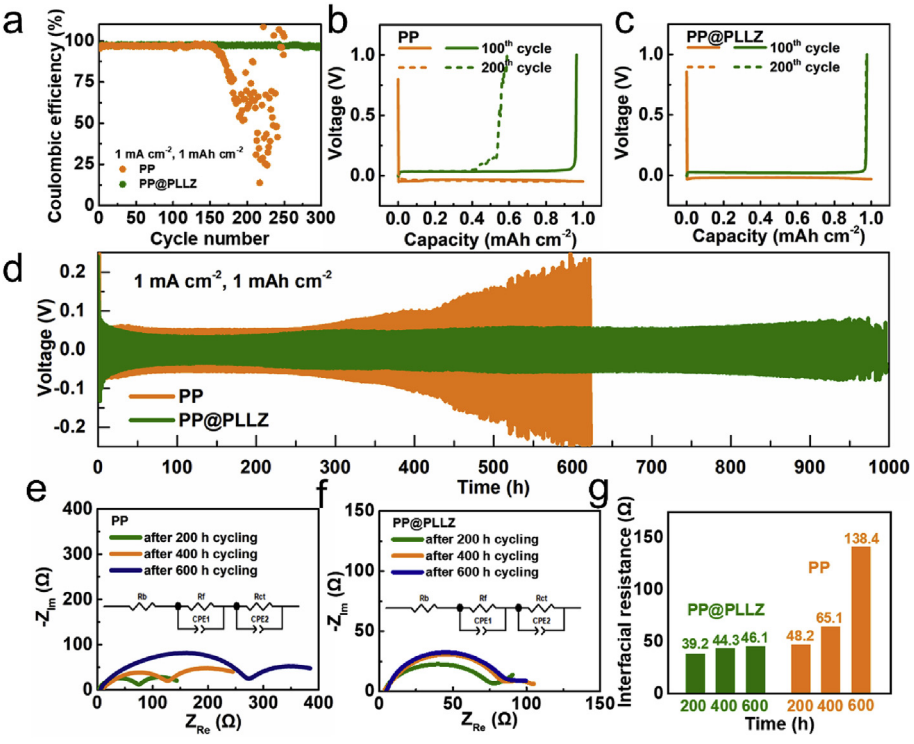

Fig. 2. a) Variations of CE with cycle numbers in Li/Cu cells under 1 mA cm^{-2} (1 mAh cm^{-2}). Charge and discharge voltage profiles of Li/Cu cells at 100th and 200th cycles with b) PP separator and c) PP@PLLZ separator. d) Voltage profiles for Li symmetric cells with different separators during galvonostatic cycles under 1 mA cm^{-2} (1 mAh cm^{-2}). e) EIS spectra of Li symmetric cells with PP separator and f) PP@PLLZ separator after 200, 400, and 600 h cycling under 1 mA cm^{-2} (1 mAh cm^{-2}). g) Interfacial resistances in Li symmetric calculated from EIS spectra.

passivation film Rf, and charge transfer resistance Rct [35]. The Rf with PP@PLLZ separator was much lower than that with PP separator (Fig. 2g). The interfacial resistance of the PP@PLLZ separator remained stable at around 46 Ω after 600 h cycling, indicating the suppressed Li dendrites and little electrolyte depletion. In contrast, the Rf with PP separator increased from 48.2 Ω to 65.1 Ω after 400 h cycling. Then, it dramatically increased to 138.4 Ω after 600 h cycling. The large fluctuations of Rf were consistent with the results of voltage hysteresis, which could be attributed to the uneven Li deposition with Li dendrite growth. The Li metal anodes before and after the cycling also confirmed the long-term stability of cells with different separators. As the SEM image shown in Fig. S8c, many sharp Li dendrites and cracks were obtained on the surface of Li metal anodes under the PP separator after cycling. However, the surface morphology of Li metal was flat with few dendrites under the PP@PLLZ separator (Fig. S8b).

The excellent long-term electrochemical stability with PP@PLLZ separator originates from the 10 μm-thick PLLZ layer covered on the PP separator, where Li^+ is uniformly redistributed by multiple highly conductive pathways. For the standard PP separator, the pores in PP filled with liquid electrolytes are considered as the only pathway for Li^+ migration. Therefore, Li^+ tends to aggregate around the holes and exhibits anisotropic distribution when passing through the PP separator. Li^+ migration can be further hindered by the free moved anions and the rapid changed local electric field, leading to an exacerbated Li^+ concentration gradient near Li anode. In contrast, as the schematic shown in Fig. 3a, the PLLZ layer shows multiple Li^+ migration pathways, redistributing the nonuniform Li^+ flux from routine PP separator, thus suppressing the formation of a large Li^+ concentration gradient.

In order to confirm the high Li^+ conductivity of PLLZ layers, EIS with various LLZTO content (0%, 10%, 20%, 50%) were tested. The PLLZ layer with 10% LLZTO (PLLZ (10%)) exhibited the highest ionic conductivity (1.4×10^{-4} S cm^{-1}) among various PPLZs at 25 °C, which was one order of magnitude larger than that of pure PVDF($LiClO_4$) (Fig. 3b and Fig. S9a). The enhanced ionic conductivity could be ascribed to the interactions between the PVDF polymer and the LLZTO particles by Lewis acid-base effect. As shown in Fig. S10, the pure PVDF($LiClO_4$) slurry was transparent. When introducing LLZTO particles, LLZTO created an alkaline-like environment to promote the partial dehydrofluorination of PVDF, thus turning the PLLZ slurry from transparent to brown. X-ray photoelectron spectroscopy (XPS) spectra were analyzed to identify the interactions between PVDF and LLZTO (Fig. 3d). The F 1s peak at 687.6 eV in PVDF($LiClO_4$) was assigned to the F–C bonding. After incorporation of LLZTO fillers, an additional peak at 684.4 eV appeared, which could be attributed to the F–Li bonding resulting from the interactions between PVDF and LLZTO [36]. Such interactions can complex with Li^+, thus effectively dissociating lithium salt and increasing Li^+ concentration for conduction. The dehydrofluorinated PVDF region by LLZTO was almost amorphous with decreased crystallinity, shown by XRD patterns in Fig. 1c. A More amorphous structure in PLLZ can promote the movement of PVDF chain segments, leading to an enhanced conductivity [23]. Besides, the PVDF/LLZTO interfaces as available sites were also in favor of Li^+ fast hopping due to percolation effect [37,38]. When the amount of LLZTO surpassed the percolation threshold (10%), the interfacial Li^+ channels were blocked, thus, in turn, decreasing the ionic conductivity (Fig. 3b).

The capability of anion immobilization of PLLZ layers can be quantified by the Li^+ transference number (t_+). A higher t_+ means more fixed anions, which can guide smooth Li^+ migration and uniform flux distribution. For PP separator, the t_+ in the ether-based electrolyte was as low as 0.2, which was consistent with previous reports (Fig. S9b and Table S1) [39]. For PP@PLLZ separator, the t_+ in the PLLZ layer was 0.66, which can effectively fix the anions to inhibit the formation of a space charge layer (Fig. 3c). The anion trapping capability could be attributed to the chemical reactions among lithium salt and LLZTO. According to XPS spectra shown in Fig. 3d, the characteristic peak at 207.7 and 208.4 eV corresponded to the ClO_4^- group in the Cl $2P_{1/2}$ and Cl $2p_{3/2}$ scans. Additional peaks at 206.7 and 205.8 eV were obtained in the PLLZ, which can be ascribed to Cl in the ClO^{3-} environment [40]. The interactions between the Li salt and LLZTO could potentially slow down the anion motion. In addition, F atoms with strong electronegativity can dissociate Li salt in the dehydrofluorinated PVDF region and enhance the Li^+ hopping along the interface, which was consistent with our XPS evidence for Li–F bonding. The Li^+ migration in the LLZTO bulk with $t_+ \approx 1$ was also beneficial for increasing the whole t_+ of PLLZ.

Full cells were assembled to evaluate the feasibility of the PP@PLLZ separator under practical conditions. The cells were cycled at various rates using $LiFePO_4$ (LFP) with a loading of ~10 mg cm^{-2} as the cathode. The rate performance of these cells can be observed in Fig. 4a; while the

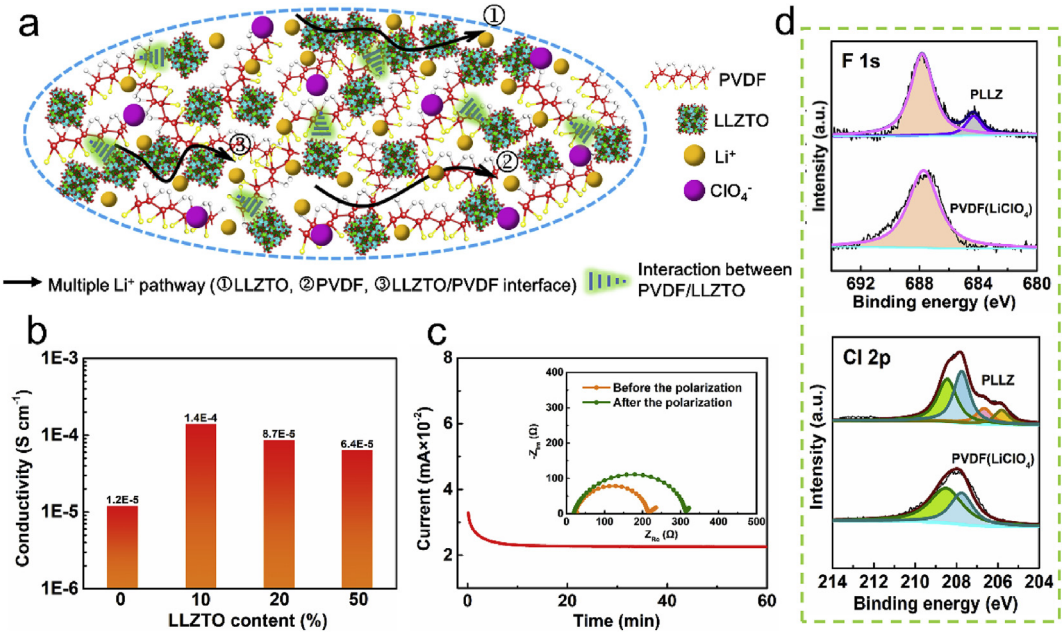

Fig. 3. a) Schematic illustration of multiple highly-conductive Li^+ transportation pathways in the PLLZ layer. b) Ionic conductivities of PLLZ layers with different LLZTO contents. c) t_+ of PLLZ (10%) layer. d) XPS spectra of F 1s and Cl 2p in PLLZ (10%) layer.

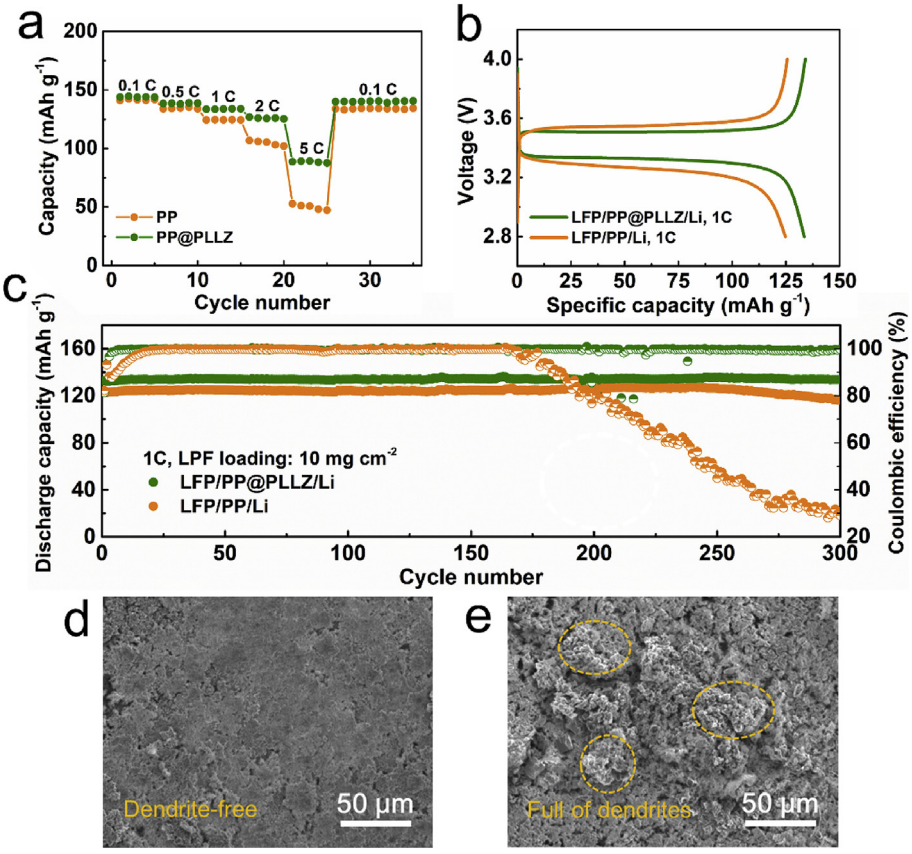

Fig. 4. a) Rate performance of LFP/Li cells with different separators. b) Charge/discharge curves and c) cycle performance of LFP/Li cells with different separators at 1C (1C = 170 mA g^{-1}). SEM images of Li metal anodes after cycling with d) PP@PLLZ separator and e) PP separator.

PP@PLLZ cells show a modest improvement over the traditional PP separator cells at a low rate (up to 1C), at rates as high as 2C and 5C (where the high current density increases the risk of harmful dendrite formation) the PP@PLLZ separator excels. Cells containing PP@PLLZ separator show an improvement in discharge capacity of 25% and 80% at 2C and 5C respectively. In addition, the cells with PP@PLLZ separators showed a lower overpotential during repeated cycling (Fig. 4b). They demonstrated almost no decreased capacity of 124 mAh $g^{-1}$with Coulombic efficiency over 99.5% even after 300 cycles at 1C (Fig. 4c and Fig. S11). The superior cycle stability resulted from the synergistic effect of uniformly redistributed Li^+ and firmly immobilized anions, which lead to the homogeneous Li^+ deposition without Li dendrite growth. The dense and smooth surface of Li metal anodes after 300 cycles was consistent with the electrochemical results (Fig. 4d). In contrast, the Coulombic efficiency of cells with PP separator began to decrease only after 160 cycles. It gradually decreased to 29.0% accompanying the capacity decay after 300 cycles. The low CE could be attributed to the sharp Li dendrite growth during the charging process, which was proved by the SEM image of Li metal beneath the routine PP separator after 300 cycles (Fig. 4e).

In order to better expand such strategy of separator modification to other coating layers, some features should be well emphasized. Firstly, the multiple highly conductive Li^+ migration pathways (including polymer, ceramic, and polymer/ceramic interface) is necessary for a coating layer to uniformly redistribute the Li^+ and guide homogenous Li^+ deposition. To prove this point, the PVDF($LiClO_4$) layer with a similar thickness of 10 μm was coated on PP separator using the same method (Figs. S12a–b). Such PVDF($LiClO_4$) layer only provided a single Li^+ transportation pathway (PVDF polymer) with much lower ionic conductivity in comparison with PLLZ layer. The CE of PVDF($LiClO_4$) in Li/Cu cells dropped to 87.7% after 100 cycles under 1 mA cm^{-2} (1 mAh cm^{-2}) cycling, while the CE of PLLZ remained over 97.5% after 300 cycles (Fig. S13). Similarly, the Li symmetrical cells with PVDF($LiClO_4$) layer demonstrated the extended voltage hysteresis with a shorter lifetime.

In order to confirm the synergistic effect of anion immobilization with multiple Li^+ migration pathways on Li dendrite suppression, a PLLZ (20%) layer was coated on PP separator to compare with the PPLZ (10%) layer (Figs. S12c–d). These two layers showed similar ionic conductivities (1.4×10^{-4} vs. 8.7×10^{-5} S cm^{-1}), while the PLLZ (20%) layer demonstrated a lower t_+ than the PLLZ (10%) layer (0.53 vs. 0.66) (Fig. 3b and Table S1). The electrochemical performance of PLLZ (20%) layer was worse than that of PLLZ (10%) due to the increased mobility of free anions (Fig. S13).

Furthermore, a moderate thickness of coating layers is also essential to achieve the optimal results. For instance, a thicker PPLZ layer with a thickness of 20 μm led to the increase in voltage polarization of Li symmetrical cells, where the Li^+ migration pathway was prolonged by the increased electrolyte thickness (Figs. S14 and S15). Besides, the cells with thin PLLZ (5 μm) layers were also confronted with the risk of the short circuit under high area capacity (3 mAh cm^{-2}) due to the deficient Li^+ redistribution and anion immobilization (Figs. S14 and S15). Therefore, multiple Li^+ migration pathways with high conductivity, high t_+, and a moderate thickness are key features for composite CSE layers on PP separators to achieve dendrite-free Li anodes with excellent electrochemical performance.

3. Conclusion

In summary, a composite-solid-electrolyte (CSE) layer consisting of PVDF and LLZTO was proposed to cover the PP separator for dendrite-free Li metal batteries. The Lewis acid-base effect between PVDF and

LLZTO enabled a superior ionic conductivity (1.4×10^{-4} S cm^{-1} at 25 °C) and a high Li^+ transference number (0.66). The multiple 3D fast Li^+ transportation pathways in the CSE layer can effectively guide Li^+ to uniformly pass through the separators. In addition, the synergistic effect of anion immobilization with Li^+ redistribution further resulted in a long-term homogeneous deposition without Li dendrite growth. Cu/Li cells with modified separators demonstrated a steady Coulombic efficiency over 97.5% for 300 cycles at 1 mA cm^{-2} (1 mAh cm^{-2}). The Li symmetric cells can stably cycle over 1000 h with a constant overpotential of 40 mV. The LFP/Li cells with a high loading of 10 mg cm^{-2} delivered no decreased capacity of ~124 mAh g^{-1} after 300 cycles at 1C, indicating the feasibility of modified separators in the practical application of Li metal batteries. This facile strategy to modify separators can be easily scalable to various composite components with different polymers and solid-state electrolyte powders, which is highly expected to show similar electrochemical performance.

Declaration of competing interest

The authors declare that they have no known competing financial interests or personal relationships that could have appeared to influence the work reported in this paper.

Acknowledgements

Hanyu Huo conceived and designed the experimental work and prepared the manuscript; Yue Chen did the XPS characterizations; Xiaona Li, Jianneng Liang, and Ruying Li helped with the SEM characterizations; Sixu Deng, Xuejie Gao, and Yang Shen helped with the fabrication of composite separators. Kieran Doyle-Davis polished the language. Xiangxin Guo, Ce-Wen Nan, and Xueliang Sun supervised the overall project. The authors would like to thank the National Key R&D Program of China (Grant No.2018YFB0104300), the National Natural Science Foundation of China (Grant No. 51771222, 51532002), the "Taishan Scholars Program", Natural Sciences and Engineering Research Council of Canada (NSERC), Canada Research Chair Program (CRC), and University of Western Ontario.

Appendix ASupplementary data

Supplementary data to this article can be found online at https://doi.org/10.1016/j.ensm.2019.12.022.

References

[1] X.B. Cheng, R. Zhang, C.Z. Zhao, Q. Zhang, Chem. Rev. 117 (2017) 10403–10473.
[2] W. Xu, J. Wang, F. Ding, X. Chen, E. Nasybulin, Y. Zhang, J.-G. Zhang, Energy Environ. Sci. 7 (2014) 513–537.
[3] X. Yang, X. Li, K. Adair, H. Zhang, X. Sun, Electrochem. Energy Rev. 1 (2018) 239–293.
[4] A.C. Luntz, B.D. McCloskey, Chem. Rev. 114 (2014) 11721–11750.
[5] Z. Peng, N. Zhao, Z. Zhang, H. Wan, H. Lin, M. Liu, C. Shen, H. He, X. Guo, J.-G. Zhang, D. Wang, Nano Energy 39 (2017) 662–672.
[6] T.-T. Zuo, X.-W. Wu, C.-P. Yang, Y.-X. Yin, H. Ye, N.-W. Li, Y.-G. Guo, Adv. Mater. 29 (2017) 1700389.
[7] X.Q. Zhang, X.B. Cheng, X. Chen, C. Yan, Q. Zhang, Adv. Funct. Mater. 27 (2017) 1605989.
[8] L. Wang, Q. Wang, W. Jia, S. Chen, P. Gao, J. Li, J. Power Sources 342 (2017) 175–182.
[9] Y. Sun, Y. Zhao, J. Wang, J. Liang, C. Wang, Q. Sun, X. Lin, K.R. Adair, J. Luo, D. Wang, R. Li, M. Cai, T.K. Sham, X. Sun, Adv. Mater. 31 (2019), e1806541.
[10] R. Zhang, X. Chen, X. Shen, X.-Q. Zhang, X.-R. Chen, X.-B. Cheng, C. Yan, C.-Z. Zhao, Q. Zhang, Joule 2 (2018) 764–777.
[11] M.F. Lagadec, R. Zahn, V. Wood, Nat. Energy 4 (2018) 16–25.
[12] P.P. Prosini, P. Villano, M. Carewska, Electrochim. Acta 48 (2002) 227–233.
[13] S. Zhang, K. Xu, T. Jow, J. Solid State Electrochem. 7 (2003) 492–496.
[14] X. Li, J. Tao, D. Hu, M.H. Engelhard, W. Zhao, J.-G. Zhang, W. Xu, J. Mater. Chem. 6 (2018) 5006–5015.
[15] H. Wu, D. Zhuo, D. Kong, Y. Cui, Nat. Commun. 5 (2014) 5193.
[16] B.-C. Yu, K. Park, J.-H. Jang, J.B. Goodenough, ACS Energy Lett. 1 (2016) 633–637.
[17] C.H. Chang, S.H. Chung, A. Manthiram, Adv. Sustain. Syst. 1 (2017) 1600034.
[18] M.H. Ryou, D.J. Lee, J.N. Lee, Y.M. Lee, J.K. Park, J.W. Choi, Adv. Energy Mater. 2 (2012) 645–650.
[19] S.S. Zhang, X. Fan, C. Wang, J. Mater. Chem. 6 (2018) 10755–10760.
[20] L. Fan, H.L. Zhuang, L. Gao, Y. Lu, L.A. Archer, J. Mater. Chem. 5 (2017) 3483–3492.
[21] J.C. Bachman, S. Muy, A. Grimaud, H.-H. Chang, N. Pour, S.F. Lux, O. Paschos, F. Maglia, S. Lupart, P. Lamp, Chem. Rev. 116 (2015) 140–162.
[22] C.-Z. Zhao, P.-Y. Chen, R. Zhang, X. Chen, B.-Q. Li, X.-Q. Zhang, X.-B. Cheng, Q. Zhang, Sci. Adv. 4 (2018), eaat3446.
[23] H.Y. Huo, B. Wu, T. Zhang, X.S. Zheng, L. Ge, T.W. Xu, X.X. Guo, X.L. Sun, Energy Storage Mater. 18 (2019) 59–67.
[24] J. Shi, Y. Xia, S. Han, L. Fang, M. Pan, X. Xu, Z. Liu, J. Power Sources 273 (2015) 389–395.
[25] H. Huo, Y. Chen, R. Li, N. Zhao, J. Luo, J.G.P. da Silva, R. Mücke, P. Kaghazchi, X. Guo, X. Sun, Energy Environ. Sci. (2019), https://doi.org/10.1039/c9ee01903k.
[26] M. He, Z. Cui, C. Chen, Y. Li, X. Guo, J. Mater. Chem. 6 (2018) 11463–11470.
[27] F. Du, N. Zhao, Y. Li, C. Chen, Z. Liu, X. Guo, J. Power Sources 300 (2015) 24–28.
[28] X. Gao, Q. Sun, X. Yang, J. Liang, A. Koo, W. Li, J. Liang, J. Wang, R. Li, F.B. Holness, A.D. Price, S. Yang, T.-K. Sham, X. Sun, Nano Energy 56 (2019) 595–603.
[29] J. Mandal, Y. Fu, A.C. Overvig, M. Jia, K. Sun, N.N. Shi, H. Zhou, X. Xiao, N. Yu, Y. Yang, Science 362 (2018) 315–319.
[30] A. Sharafi, S. Yu, M. Naguib, M. Lee, C. Ma, H.M. Meyer, J. Nanda, M. Chi, D.J. Siegel, J. Sakamoto, J. Mater. Chem. 5 (2017) 13475–13487.
[31] S. Yang, J. Gu, Y. Yin, J. Appl. Polym. Sci. 135 (2018) 45825.
[32] B.D. Adams, J. Zheng, X. Ren, W. Xu, J.-G. Zhang, Adv. Energy Mater. 8 (2018) 1702097.
[33] C. Li, S. Liu, C. Shi, G. Liang, Z. Lu, R. Fu, D. Wu, Nat. Commun. 10 (2019).
[34] R. Xu, Y. Xiao, R. Zhang, X.B. Cheng, C.Z. Zhao, X.Q. Zhang, C. Yan, Q. Zhang, J.Q. Huang, Adv. Mater. (2019), e1808392.
[35] T. Zhang, N. Imanishi, S. Hasegawa, A. Hirano, J. Xie, Y. Takeda, O. Yamamoto, N. Sammes, J. Electrochem. Soc. 155 (2008) A965.
[36] Y. Sun, X. Zhan, J. Hu, Y. Wang, S. Gao, Y. Shen, Y.T. Cheng, ACS Appl. Mater. Interfaces 11 (2019) 12467–12475.
[37] H. Huo, Y. Chen, J. Luo, X. Yang, X. Guo, X. Sun, Adv. Energy Mater. 9 (2019) 1804004.
[38] H. Huo, N. Zhao, J. Sun, F. Du, Y. Li, X. Guo, J. Power Sources 372 (2017) 1–7.
[39] C.Z. Zhao, X.Q. Zhang, X.B. Cheng, R. Zhang, R. Xu, P.Y. Chen, H.J. Peng, J.Q. Huang, Q. Zhang, Proc. Natl. Acad. Sci. U. S. A. 114 (2017) 11069–11074.
[40] W.E. Morgan, J.R. Van Wazer, W.J. Stec, J. Am. Chem. Soc. 95 (1973) 751–755.